Auchter, N.C., et al., 2020, Intrabasinal sediment recycling from detrital strontium isotope stratigraphy: Geology, v. 48, https://doi.org/10.1130/G47594.1

Supplementary Material

A) Backscattered Electron Scanning Electron Microscopy Screening

Representative samples were inspected via backscattered electron scanning electron microscopy (BSE-SEM) in order to evaluate the quality of preservation and screen for elemental composition (Suppl. Fig. B). Samples were analyzed using a Hitachi TM3000 tabletop thermionic (tungsten filament source) SEM at the Virginia Tech Department of Geosciences following the procedures outlined in Muscente and Xiao (2015). We used backscatter electron collection (BSE) for topographic imaging of the sample and the Everhart-Thornley detector applying a negatively biased Faraday cage [EDS(-)] for compositional imaging (Muscente and Xiao, 2015). Topographic inspection with BSE imaging allows us to evaluate preservation integrity of the sample surface and identify any potential secondary mineralization, diagenetic dissolution, or other physical defects (McArthur et al., 1994). Samples with abundant pitting, observable secondary mineralization, or minimal shell material were rejected. Element mapping using EDS(-) imaging allows us to screen for compositional integrity of the sample. A given sample should have complete surficial coverage of calcium, carbon, and oxygen with approximate ratio of 1:1:3 appropriate for $CaCO_3$ (Suppl. Fig. B). Samples with incomplete elemental coverage on the imaged shell surface or significantly skewed elemental ratios were interpreted to be replaced shell material or otherwise diagenetically altered and were rejected.

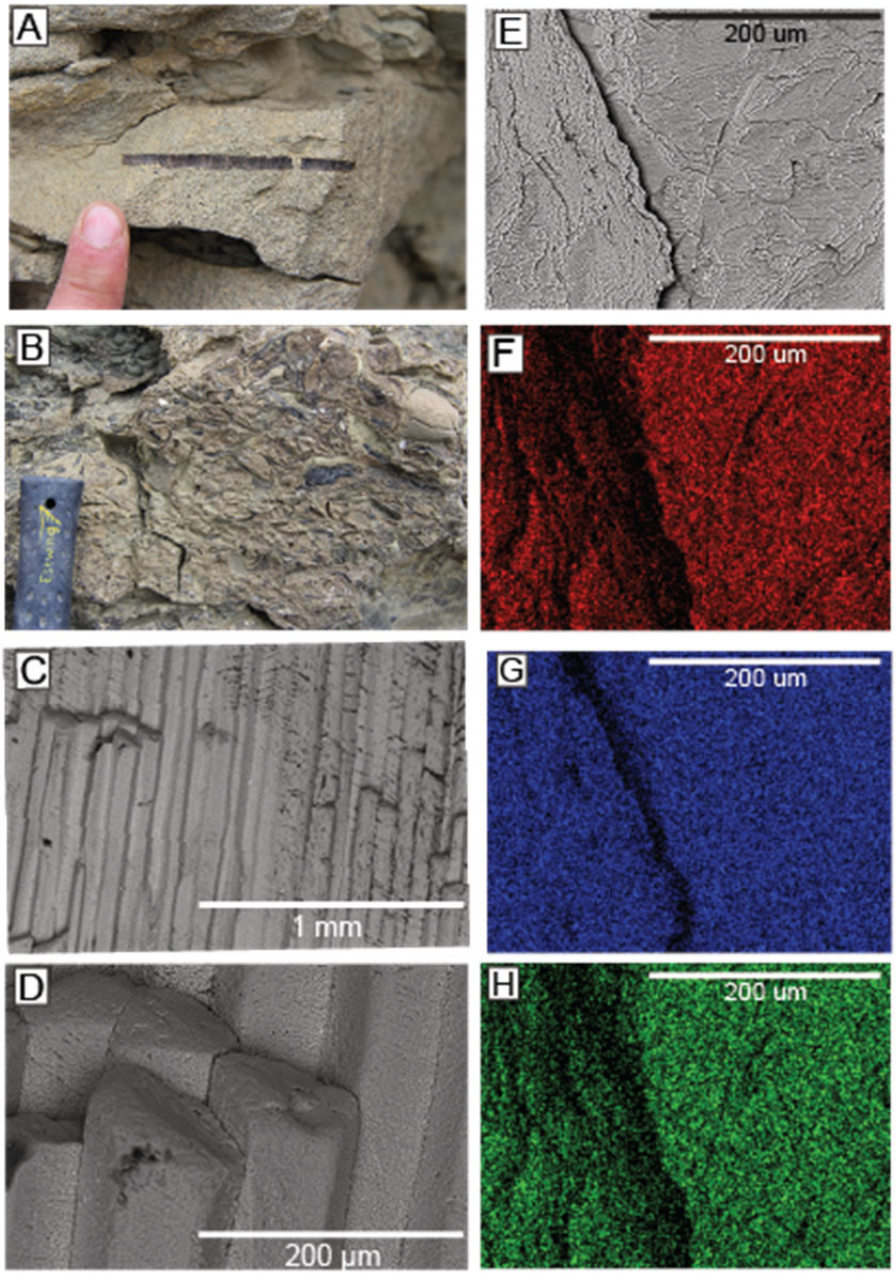

Suppl. Figure A: A-B) example of sample collection for inoceramid (A) and oyster (B) shell fragments. C-D) BSE-SEM images of inoceramid fragment showing integrity of sample surface with minimal pitting or secondary mineralization. E-H) BSE-SEM € and EDS(-) images (F-H) of an oyster fragment showing elemental composition of sample surface for oxygen (F), calcium (G), and carbon (H).

B) Trace Elemental Analysis Screening

For samples with sufficient amounts of shell material available (125 samples; 85% of total) we ground additional material for trace element analysis. We dissolved 50 mg of ground carbonate powder in trace metal grade acetic acid. Trace element concentrations were measured for Ca, Fe, Mg, Mn, and Sr at the Virginia Tech Soil Testing Lab using inductively coupled plasma spectroscopy (ICP) analysis. Measured concentrations allowed for screening and rejection of samples with anomalously low concentrations of Ca or Sr and/or anomalously high concentrations of common replacement cations such as Fe, Mg, and Mn (McArthur et al., 1994), which indicate diagenetic alteration and cation replacement of Sr (Suppl. Fig. C).

Previous strontium isotope stratigraphy studies have suggested acceptable element concentrations for Fe, Mg, Mn and Sr to guide evaluation of measured results (McArthur et al., 1994); however, there is no definitive threshold for element concentrations. In order to develop an element concentration baseline for this study we compared the Sr, Fe, and Mn concentrations of acceptable and aberrant $^{87}Sr/^{86}Sr$ ratios (Suppl. Fig. C). Based on these comparisons we established concentration thresholds for Sr (>350 ppm), Fe (<1000 ppm), and Mn (<600 ppm). While these are higher than other published thresholds (e.g. Fe <500 ppm and Mn <300 ppm from McArthur et al., 1994), we find the internal consistency of acceptable results and distinct separation between measured Fe and Mn concentrations associated with acceptable and aberrant $^{87}Sr/^{86}Sr$ ratios to be sufficient for screening sample integrity.

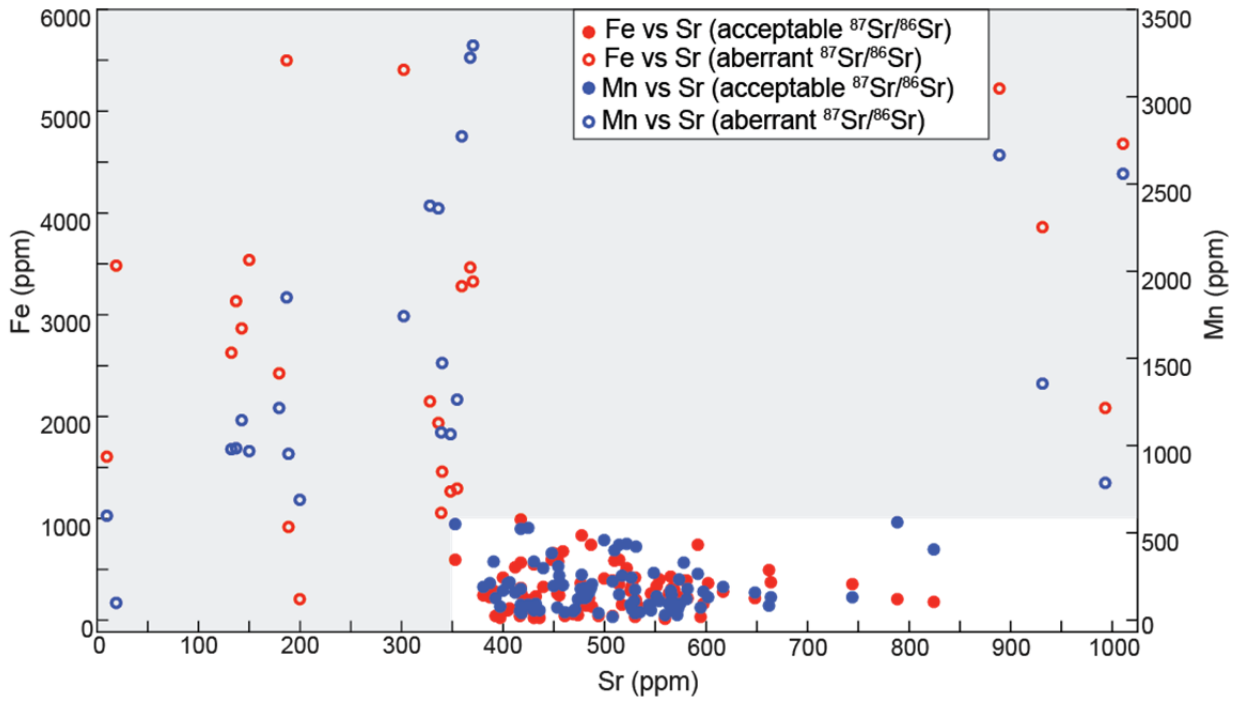

Suppl. Figure B: Trace element analysis demonstrating the disparity between DSIS samples producing acceptable $^{87}Sr/^{86}Sr$ ratios and those that did not. The gray zone indicates thresholds for unacceptable concentrations of Fe, Mn, and Sr.

C) Strontium Isotope Measurements

Approximately 1 mg of carbonate sample powder was dissolved in ultrapure 0.5 M acetic acid in acid washed micro centrifuge tubes. The supernatant was decanted following centrifugation to ensure no undissolved detrital material was loaded onto the Sr extraction columns. Sr was separated from other cations using SrSpec cation extraction resin. Three aliquots of the carbonate standard E&A was processed in parallel with the unknowns. Sr isotope analyses of 60 unknowns were bracketed by 18 analyses of Sr isotope standard NBS987. Beam intensities were monitored using the voltage on mass 86, which ranged from 0.3–3.8 V for the unknowns and was ~1.5 V for the standard. Samples were aspirated at 100 μ l/min through a PFA nebulizer and the resulting aerosol was introduced to the plasma using a quartz glass Scott-type spray chamber and a quartz injector. Nickel sampler and skimmer cones were used at the interface to the inductively coupled plasma mass spectrometer (ICPMS). The instrument was tuned for maximum sensitivity and beam stability. The voltages of masses 83, 84, 85, 86, 87, 88, and 90 were measured for 35 cycles of 8 s, and the average voltage was calculated after a 2-sigma outlier test. Before each analysis baseline voltages were measured for 30 seconds and a baseline correction was applied for all masses. Replicate analysis of Sr isotope standard NBS 987 yielded 0.710288 ± 0.000013 (2s, n=18). All $^{87}Sr/^{86}$ Sr ratios have been normalized to the accepted value of NBS987 = 0.710248 (McArthur et al., 1994). The three E&A standards yielded 0.708021 ± 0.000022 (2s, n=3).

Instrumental mass fractionation was corrected by normalizing to $^{86}Sr/^{88}Sr = 0.1194$ using an exponential law. Potential isobaric interferences arise from krypton (Kr) and rubidium (Rb), which is derived from the argon supply and suboptimal purification on the cation exchange columns, respectively. Mass 83 is monitored for krypton levels and mass 85 is monitored for Rb levels.

Voltages on mass 83 are less than 0.06 mV, which would contribute less than 0.09 mV to mass 86. For most samples the level of Kr contributes less than 0.003% of the voltage measured on mass 86. Sample PV DT 30 had a low signal (~0.3 V on 86) and the contribution of Kr to the measured voltage on mass 86 is 0.015%. An interference correction for Kr has been applied to the data, using an $^{83}Kr/^{86}Kr$ ratio of 0.66474, correcting for mass fractionation by normalizing to $^{86}Sr/^{88}Sr = 0.1194$ using an exponential law, and assuming mass discrimination behavior of Kr is identical to Sr.

Voltages on mass 85 range from 0.01–0.4 mV, which would contribute 0.004–0.15 mV to mass 87. For most samples the level of Rb contributes less than 0.001% of the voltage measured on mass 87. For the smallest sample PV DT 30 the contribution is 0.08%. An interference correction for Rb has been applied to the data, using an $^{85}Rb/^{87}Rb$ ratio of 2.59, correcting for mass fractionation by normalizing to $^{86}Sr/^{88}Sr = 0.1194$ using an exponential law, and assuming mass discrimination behavior of Rb is identical to Sr. A procedural blank was measured semi-quantitatively by voltage comparison on the Neptune MC-ICPMS. A 500 ppb solution of NBS 987 yielded 12.8 V on mass 88. The procedural blank solution was reconstituted in 800 ml of 2% HNO3 and produced 0.005 V on mass 88. The mass of Sr in the procedural blank is 140 pg.

D) Histogram and Kernel Density Estimate

The histogram is binned at 1-Myr intervals and the overlying kernel density estimate curve uses the "sj" (Sheather & Jones, 1991; Journal of Royal Statistical Society B, 53, pp. 683-690) smoothing parameter that is the default in the open-source software R (https://cran.r-project.org/), which is what we used to create this plot. The "sj" method selects the bandwidth using pilot estimation of derivatives and minimizes estimates of the mean integrated squared error.

Supplementary Table Captions

Suppl. Table A: Data and results table indicating sample name, number, location code linked to locations in Fig 2, batch number (1-3), and specimen type for each sample. Analytical results, uncertainties, and numerical ages are shown for each sample. Trace element concentrations were measured for Ca, Fe, Mg, Mn, and Sr via ICP analysis, $^{86}Sr/^{88}Sr$ was measured via ICPMS and normalized NBS987 = 0.710248, and numerical ages were derived from the LOWESS look-up table. Where trace element results are absent there was not enough material to run the analysis. Where $^{86}Sr/^{88}Sr$ is not reported the analysis was not run because the sample did not pass screening. Where error and numerical age is not calculated, the $^{86}Sr/^{88}Sr$ was deemed aberrant and was rejected.

References (Supplementary)

McArthur, J.M., Kennedy, W.J., Chen, M., Thirlwall, M.F., and Gale, A.S., 1994, Strontium isotope stratigraphy for the Late Cretaceous: Direct numerical calibration of the Sr isotope curve based on the US Western Interior, Palaeogeography, Palaeoclimatology, Palaeoecology, v. 108, p. 95-119, https://doi.org/10.1016/0031-0182(94)90024-8.

Muscente, A.D. and Xiao, S., 2015, Resolving three-dimensional and subsurficial features of carbonaceous compressions and shelly fossils using backscattered electron scanning electron microscopy (BSE-SEM), Palaios, v. 30, p. 462-481, https://doi.org/10.2110/palo.2014.094.

Sheather, S.J. and Jones, M.C., 1991, A reliable data-based bandwidth selection method for kernel density estimation, Journal of the Royal Statistical Society: Series B (Methodological), v. 53, p. 683-690, https://doi.org/10.1111/j.2517-6161.1991.tb01857.x.